CHEMISTRY OF MATERIALS

pubs.acs.org/cm

Article

Polymerization-Induced Self-Assembly Toward Micelle-Crosslinked Tough and Ultrastretchable Hydrogels

Linlin Fan, Zhong Zeng, Ruixue Zhu, Aiping Liu,* Hailong Che,* and Meng Huo*

Cite This: *Chem. Mater.* 2022, 34, 6408−6419

Read Online

ACCESS | Metrics & More | Article Recommendations | Supporting Information

ABSTRACT: As a promising class of tough and ultrastretchable hydrogels, micelle-crosslinked hydrogels have been restrained by the scarcity of micellar crosslinkers with a high concentration, controlled nanostructure, and uniform size distribution. Herein, polymerization-induced self-assembly (PISA) was demonstrated to be a general and powerful platform for micellar crosslinkers, affording micelle-crosslinked hydrogels with tailorable chemical structures, mechanics, and functionality. Poly(*N*,*N*-dimethylacrylamide)-*b*-poly(diacetone acrylamide) (PDMAc-*b*-PDAAM) micellar crosslinkers with a controlled nanostructure and uniform size distribution were prepared via PISA and one-step post-polymerization modification at high concentrations. Copolymerization of these micellar crosslinkers with acrylamide generated tough and ultrastretchable hydrogels, whose mechanical properties were found correlated with the concentration, nanostructure, and chemical composition of the micelles. The energy dissipation mechanism of these micelle-crosslinked hydrogels was analyzed via cyclic mechanical tests and stress relaxation experiments. The general feasibility of PISA toward micelle-crosslinked hydrogels was verified by systematic evaluation of both aqueous (including 2-methoxyethyl acrylate, tetrahydro-2-furanylmethyl acrylate, and 4-hydroxybutyl acrylate) and alcoholic (including benzyl methacrylate, lauryl methacrylate, styrene, and benzyl acrylate) PISA formulations, producing hydrogels with diverse chemical structures, mechanics, and functionalities depending on the micellar crosslinkers. The modularity of this strategy was further demonstrated by the fabrication of fluoro-functionalized hydrogels with fluoro-containing micellar crosslinkers. This strategy has significantly enlarged the scope and application of micelle-crosslinked hydrogels.

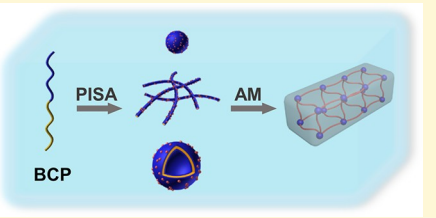

INTRODUCTION

Hydrogels are fascinating soft materials consisting of physically or chemically crosslinked polymers that are swollen by water. The inherently tissue-like nature makes hydrogels excellent candidates for regenerative medicine,[1,2] soft robotics,[3] sensors,[4] and wearable electronics.[5] Unfortunately, conventional synthetic hydrogels are weak and fragile due to their structural inhomogeneity and incapable of effective energy dissipation, which impedes their practical applications. Integrating an energy dissipation mechanism into hydrogel networks is the central principle for designing tough hydrogels.[6−9] Guided by this principle, several strategies have been proposed, including interpenetrating networks,[10−12] nanocomposite hydrogels,[13−15] and hydrogels crosslinked by polymer colloids.[16,17] Among them, crosslinking based on polymeric micelles has been demonstrated to be a reliable route to ultrastretchable and tough hydrogels.[16,18−21] The reversible deformation of soft micelles and the dynamic hydrophobic association within micelles guarantee effective energy dissipation throughout the hydrogels.[22−24] To achieve micelle-crosslinked hydrogels with high strength, toughness, and elongation, micellar crosslinkers with a high concentration, controlled size, and uniform size distribution are generally required. For example, Fu et al. prepared high-concentration micellar crosslinkers (ca. 75 mg mL^{-1}) based on diacrylated Pluronic F127 and copolymerized them with acrylamide (AM), generating a tough hydrogel with a fracture stress (σ_b) of 276 kPa and a fracture strain (ε_b) of 2265%.[25] Yang et al. further optimized the size dispersity of the Pluronic F127 crosslinker, yielding hydrogels with homogeneous crosslinking. Correspondingly, the σ_b and ε_b of the hydrogel increased to 0.94 MPa and 2950%, respectively.[26] The excellent tensile property thus makes micelle-crosslinked hydrogels promising candidates in wound healing,[27,28] actuators,[29] and wearable electronics.[30] Despite these achievements, micellar crosslinkers with a tailor-made nanostructure and uniform size dispersity are still difficult to achieve with conventional self-assembly techniques due to their laborious post-polymerization steps and complex kinetic factors, such as the mobility of the polymer chains, the nature of the common solvent, and even the rate of water addition.[31]

Polymerization-induced self-assembly (PISA) offers an efficient approach to polymeric assemblies with a high concentration, controlled nanostructure, and uniform disper-

Received: April 2, 2022
Revised: June 21, 2022
Published: July 5, 2022

https://doi.org/10.1021/acs.chemmater.2c01001
Chem. Mater. 2022, 34, 6408−6419

Scheme 1. Schematic Illustration of PISA for Micelle-Crosslinked Tough and Ultrastretchable Hydrogels

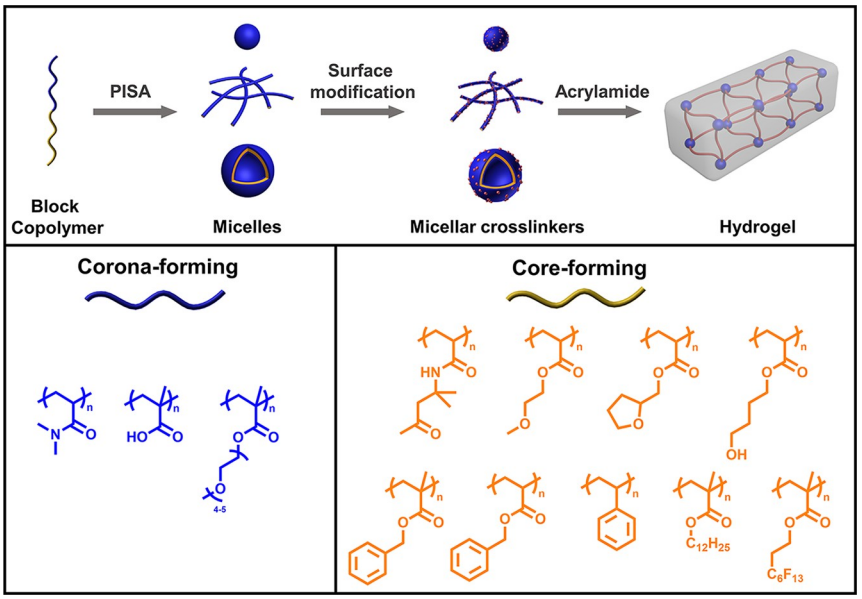

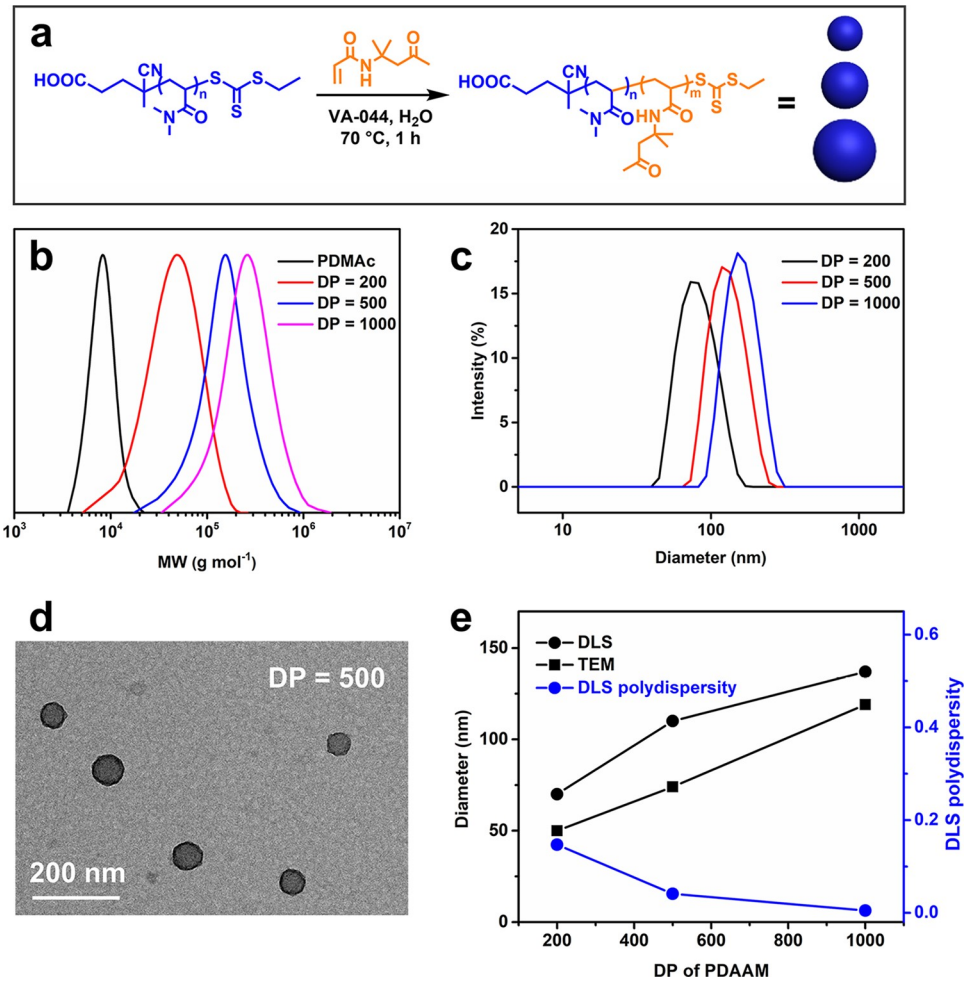

Figure 1. Aqueous PISA of PDMAc-*b*-PDAAM. (a) Fabrication of PDMAc-*b*-PDAAM micelles via RAFT dispersion polymerization of DAAM with PDMAc as the macro-CTA. Solids content = 20 wt %. (b) SEC and (c) DLS characterization of the PDMAc-*b*-PDAAM copolymers. The theoretical degrees of polymerization (DP) of PDAAM are 200, 500, and 1000. (d) Representative TEM image of $PDMAc_{100}$-*b*-$PDAAM_{500}$ micelles. (e) Diameter and DLS polydispersity of the micelles vs DP of PDAAM.

https://doi.org/10.1021/acs.chemmater.2c01001
Chem. Mater. 2022, 34, 6408−6419

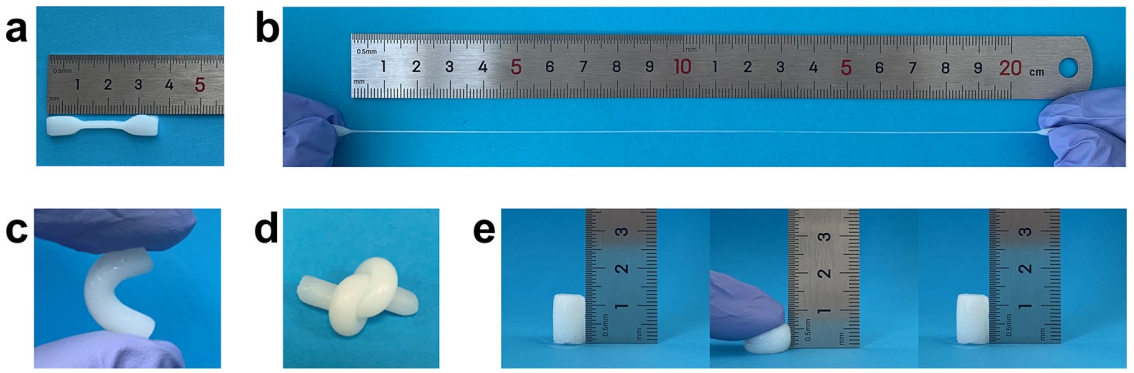

Figure 2. Photographs of the $PDMAc_{100}$-*b*-$PDAAM_{500}$ micelle-crosslinked polyacrylamide hydrogels under different deformations: (a) original, (b) stretched, (c) bent, (d) knotted, and (e) compressed. c_{AM} = 5 mol L^{-1} and $c_{micelle}$ = 0.71 mmol L^{-1}.

sity.[32−37] In a typical PISA system, a solvophilic block is chain-extended by a solvophobic block via controlled dispersion or emulsion polymerization.[36,38] Therefore, it enables simultaneous growth of amphiphilic copolymers and their in situ self-assembly in selective solvents. Polymeric assemblies with controlled size and morphology, including spherical micelles, wormlike micelles, and vesicles, could be readily prepared via rational design of the chain lengths of both solvophilic and solvophobic blocks.[39−42] Compared with the conventional self-assembly techniques, PISA enables simplifying influencing factors during the preparation of polymer assemblies, and the concentration of polymer assemblies could be as high as 50 wt %. In this work, a series of micellar crosslinkers with a tailored chemical composition, nanostructure, and functionality are rationally designed and prepared by PISA and one-step post-polymerization modification (Scheme 1). Copolymerization of these micellar crosslinkers with AM produces tough and ultrastretchable hydrogels, whose mechanical performances are assessed in terms of their tensile, compressive, and fatigue resistance properties. The mechanical properties of these hydrogels are further correlated with the concentration, nanostructure, and chemical composition of the micelles, and the energy dissipation mechanism is analyzed via stress relaxation and cyclic mechanical tests. The general feasibility of PISA toward micelle-crosslinked hydrogels is systematically evaluated with multiple aqueous and alcoholic PISA formulations. Furthermore, the modularity of this strategy is assessed with the fabrication of fluoro-functionalized hydrogels using fluoro-containing micellar crosslinkers.

RESULTS AND DISCUSSION

Aqueous PISA for Micellar Crosslinkers of Controlled Size. To demonstrate the benefits of PISA in fabricating micellar crosslinkers for tough hydrogels, polymeric micelles of controlled size were first prepared via a typical aqueous PISA system,[43,44] which used poly(*N*,*N*-dimethylacrylamide) ($PDMAc_{100}$, M_n = 7800 g mol^{-1}, $Đ$ = 1.09) as the macro-chain-transfer agent (macro-CTA) and poly(diacetone acrylamide) (PDAAM) as the core-forming block (Figure 1a−e). RAFT polymerization was used due to its good tolerance to a diverse range of functional groups, including carboxylic acid, hydroxyl, azide, epoxy, etc.[45,46] In our study, carboxylic acid-functionalized RAFT agent, 4-cyano-4-(ethylthiocarbonothioylthio) pentanoic acid (CETP), was leveraged to anchor a carboxylic group onto the chain end of the PDMAc block (Figure S1). Chain-extension of PDMAc with diacetone acrylamide (DAAM) via RAFT dispersion polymerization generates PDMAc-*b*-PDAAM copolymers, which self-assemble in situ into micelles with the carboxylic acid group on their surface (Figure 1a). As the molar ratio of DAAM/PDMAc varies from 200 to 1000, the molecular weight of PDMAc-*b*-PDAAM copolymers increases from 37.1 to 210 kDa, while their dispersity values remain low ($Đ$ <1.45) (Figure 1b and Table S1). All these PISA formulations generate spherical micelles, whose hydrodynamic size increases from 69.5 to 137 nm as the PDAAM block grows (Figure 1c−e and Figure S2). Notably, all these micelles possess a narrow size distribution, with their polydispersity index (PDI) lower than 0.15, which is critical to the formation of uniform hydrogel networks.[26]

Micellar crosslinkers with polymerizable vinyl groups were readily synthesized by EDC coupling of *N*-(2-aminoethyl)-methacrylamide hydrochloride (AEMA) with carboxylic acid groups on the surface of PDMAc-*b*-PDAAM micelles (Figure S3). After the coupling reaction, ^{1}H NMR spectroscopy revealed the characteristic peaks of vinyl groups at 5.6 and 5.3 ppm, confirming the successful modification of the micelles (Figure S4). Almost 100% modification efficiency is achieved for all the PDMAc-*b*-PDAAM micelles. Dynamic light scattering (DLS) and transmission electron microscopy (TEM) characterization show negligible change in micellar size, morphology, and polydispersity, which confirm the minimal influence of surface modification on the colloidal stability of the PDMAc-*b*-PDAAM micelles (Figure S5). On the contrary, end-group modification was reported to have a significant influence on micellar stability and pH-responsiveness of the commercial Pluronic F127 micelles.[26]

Fabrication and Mechanical Properties of the Micelle-Crosslinked Hydrogels. Free-radical copolymerization of AM with the PDMAc-*b*-PDAAM micellar crosslinkers produced hydrogels with superior mechanical properties. The as-prepared hydrogels could be bent, knotted, and compressed and could even endure at least 1600% strain (Figure 2a−e).

The mechanics of the as-prepared micelle-reinforced hydrogels could be readily regulated by the concentration of AM (c_{AM}) and micelle ($c_{micelle}$). As c_{AM} increases from 2 to 8 mol L^{-1}, the hydrogels show a significant increase in tensile strength, Young's modulus, and toughness (Figure S6). Especially, the σ_b and ε_b of the hydrogel with c_{AM} = 8 mol L^{-1} reach 852 kPa and 2080%. The work of extension is as high as 5.88 MJ m^{-3}, suggesting excellent toughness. Moreover, these hydrogels remain undamaged under 98% compressive strain, with the compressive stress at 98% strain ($\sigma_{c,98\%}$) increasing with c_{AM}. As a comparison, the chemically crosslinked polyacrylamide hydrogel shows a much lower ε_b

https://doi.org/10.1021/acs.chemmater.2c01001
Chem. Mater. 2022, 34, 6408−6419

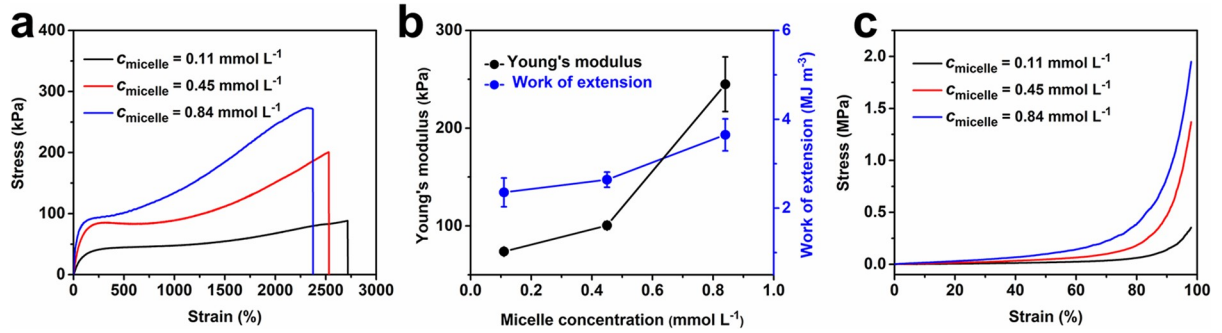

Figure 3. Tensile and compressive performances of the hydrogels prepared at different PDMAc$_{100}$-*b*-PDAAM$_{1000}$ micelle concentrations. c_{AM} = 5 mol L^{-1}. $c_{micelle}$ = 0.11, 0.45, and 0.84 mmol L^{-1}. (a) Tensile stress−stain curves, (b) Young's modulus and work of extension, and (c) compressive stress−strain curves of the hydrogels.

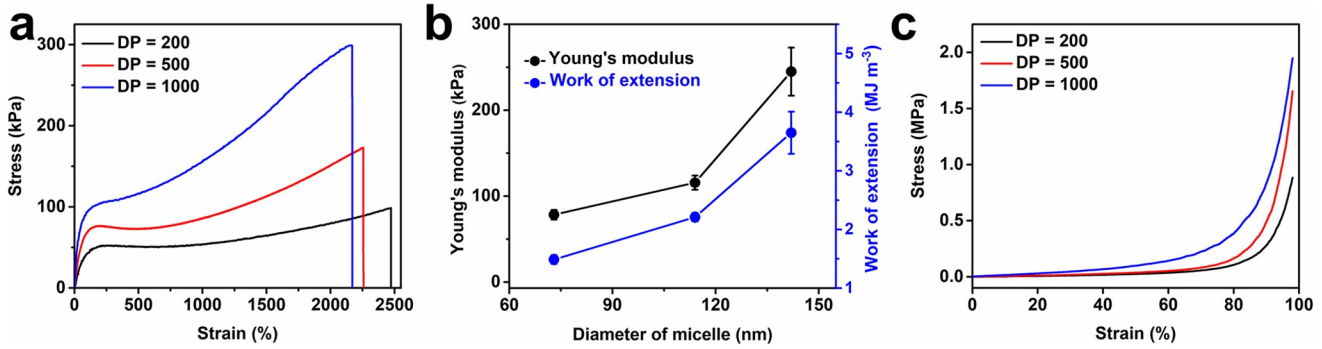

Figure 4. Tensile and compressive performances of the hydrogels prepared using PDMAc$_{100}$-*b*-PDAAM micellar crosslinkers with varying DP of PDAAM. c_{AM} = 5 mol L^{-1} and $c_{micelle}$ = 0.84 mmol L^{-1}. (a) Tensile stress−stain curves, (b) Young's modulus and work of extension, and (c) compressive stress−strain curves of the hydrogels.

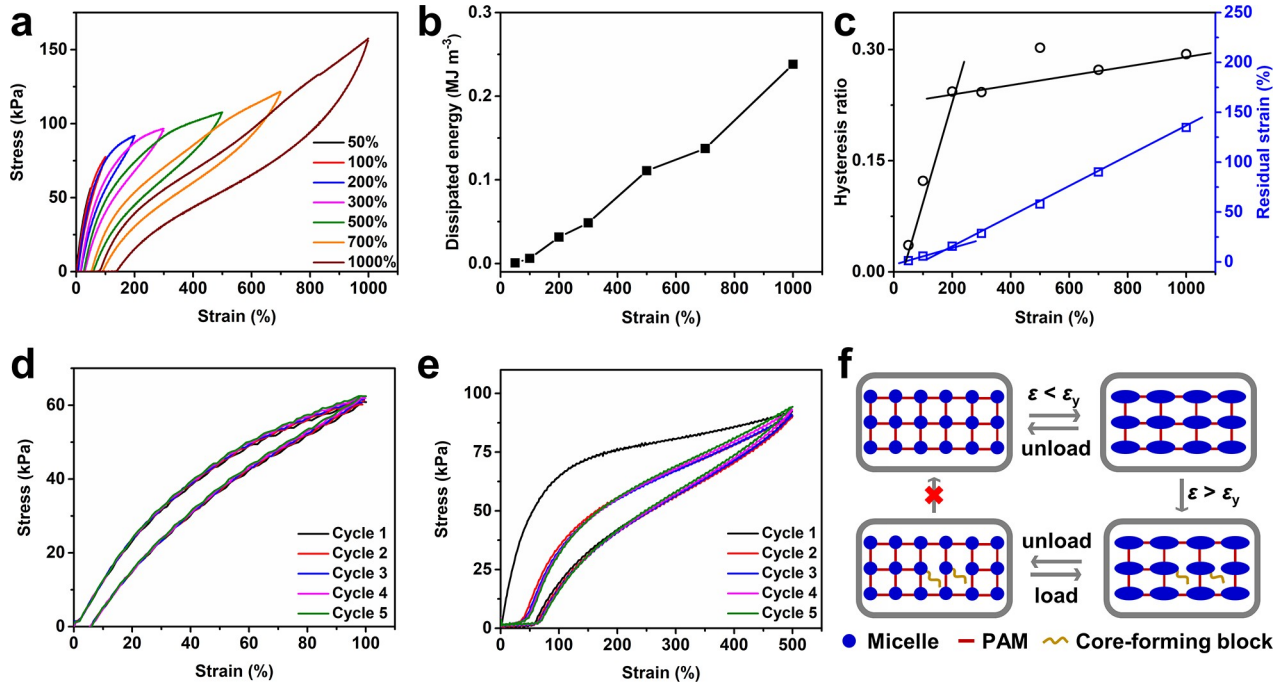

Figure 5. Cyclic tensile tests of the hydrogel crosslinked with the PDMAc$_{100}$-*b*-PDAAM$_{1000}$ micellar crosslinker. c_{AM} = 5 mol L^{-1} and $c_{micelle}$ = 0.45 mmol L^{-1}. (a) Cyclic tensile stress−strain curves, (b) dissipated energy, and (c) hysteresis ratio and residual strain of the hydrogel. The test was performed without time intervals between each cycle. (d and e) Cyclic tensile tests under (d) 100% strain and (e) 500% strain. Between each cycle, the hydrogel was rested for 5 min. (f) Schematic illustration of the dissipative process during cyclic tensile under 100 and 500% strains.

and toughness, indicating the effective toughening of hydrogels with micellar crosslinkers (Figure S7).

Subsequently, the effect of $c_{micelle}$ on the mechanical properties of hydrogels was assessed at c_{AM} = 5 mol L^{-1}

https://doi.org/10.1021/acs.chemmater.2c01001
Chem. Mater. 2022, 34, 6408−6419

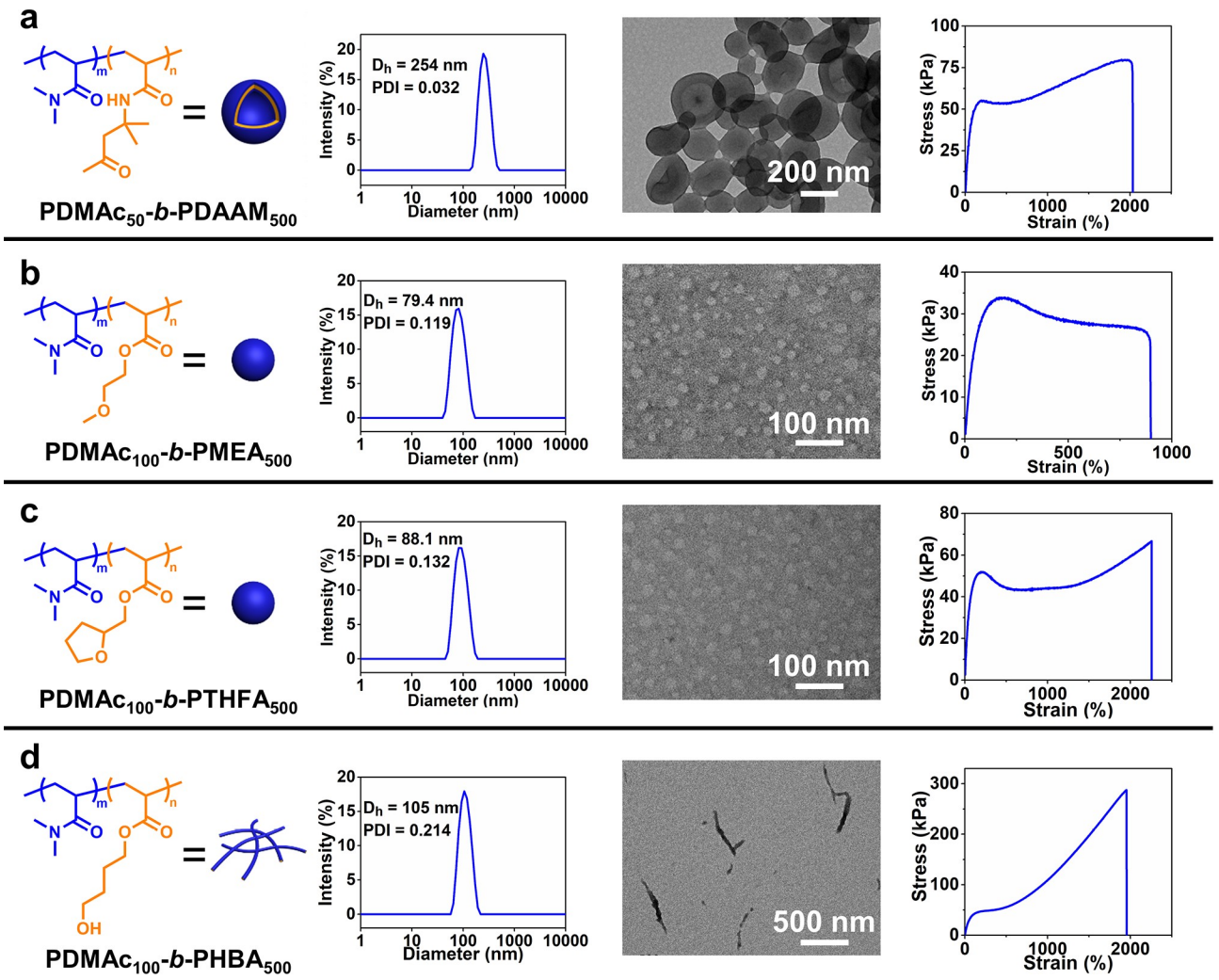

Figure 6. Summary of the aqueous PISA formulations for micelle-crosslinked tough and ultrastretchable hydrogels. PISA of (a) $PDMAc_{50}$-*b*-$PDAAM_{500}$, (b) $PDMAc_{100}$-*b*-$PMEA_{500}$, (c) $PDMAc_{100}$-*b*-$PTHFA_{500}$, and (d) $PDMAc_{100}$-*b*-$PHBA_{500}$ for micelle-crosslinked hydrogels. For each PISA formulation, the hydrodynamic size and morphology of the assemblies were characterized by DLS and TEM, and the mechanical property of the as-prepared hydrogel was characterized by a tensile test.

(Figure 3a–c). As expected, the crosslink density increases with $c_{micelle}$, resulting in a greater stiffness, strength, and toughness. As $c_{micelle}$ increases from 0.11 to 0.84 mmol L^{-1}, σ_b increases from 88.4 to 272 kPa, whereas ε_b declines slightly from 2720 to 2380%. According to the nominal stress–strain curves, the Young's modulus and work of extension increase from 73.8 kPa and 2.35 MJ m^{-3} to 245 kPa and 3.65 MJ m^{-3}, respectively. Similarly, the compressive strength of these hydrogels exhibits an increasing trend with $c_{micelle}$.

Because micellar crosslinkers with controlled size and narrow size distribution could be readily prepared via PISA, the correlation of the micelle nanostructure to the mechanical properties of micelle-crosslinked hydrogels could therefore be assessed. Hydrogels were prepared with c_{AM} = 5 mol L^{-1} and $c_{micelle}$ = 0.84 mmol L^{-1}, whereas the size of the micelles varied from 73.2 to 142 nm. Interestingly, tensile tests show that as the micellar size increases, the Young's modulus and work of extension increase from 78.4 kPa and 1.49 MJ m^{-3} to 245 kPa and 3.65 MJ m^{-3}, respectively (Figure 4a–c). Likewise, compressive tests show an increasing trend of $\sigma_{c,98\%}$ with the increase in the micellar diameter. Scanning electron microscopy (SEM) reveals that the average pore size of these hydrogels diminishes from ca. 86 to 10 μm as the size of micelles increases, suggesting the increase in crosslinking density (Figure S8). Based on the mechanical tests and SEM characterization, we speculate that the enhanced Young's modulus and toughness may be correlated with the branch functionality (f) of the hydrogel network. As has been revealed in PISA, the mean aggregation number (N_{agg}) of polymeric assemblies increases with the DP of the hydrophobic block,[47−49] which means that the PDMAc-*b*-PDAAM micellar crosslinkers with a higher DP of PDAAM have more vinyl groups per sphere. As a consequence, the corresponding hydrogel has a higher branch functionality, leading to a denser network and enhanced mechanical properties.[50]

The dissipative process of the micelle-crosslinked hydrogel was quantitatively assessed by cyclic mechanical tests. As shown in Figure 5a, the hydrogel sample was cyclically stretched to predetermined maximum strains and immediately returned to its original length. Each loading–unloading cycle shows a hysteresis loop, with the dissipated energy (U_{hys}) increasing with the maximum strain (Figure 5b). According to the Lake-Thomas mechanism, U_{hys} is related to the crosslink by eq 1:

https://doi.org/10.1021/acs.chemmater.2c01001
Chem. Mater. 2022, 34, 6408−6419

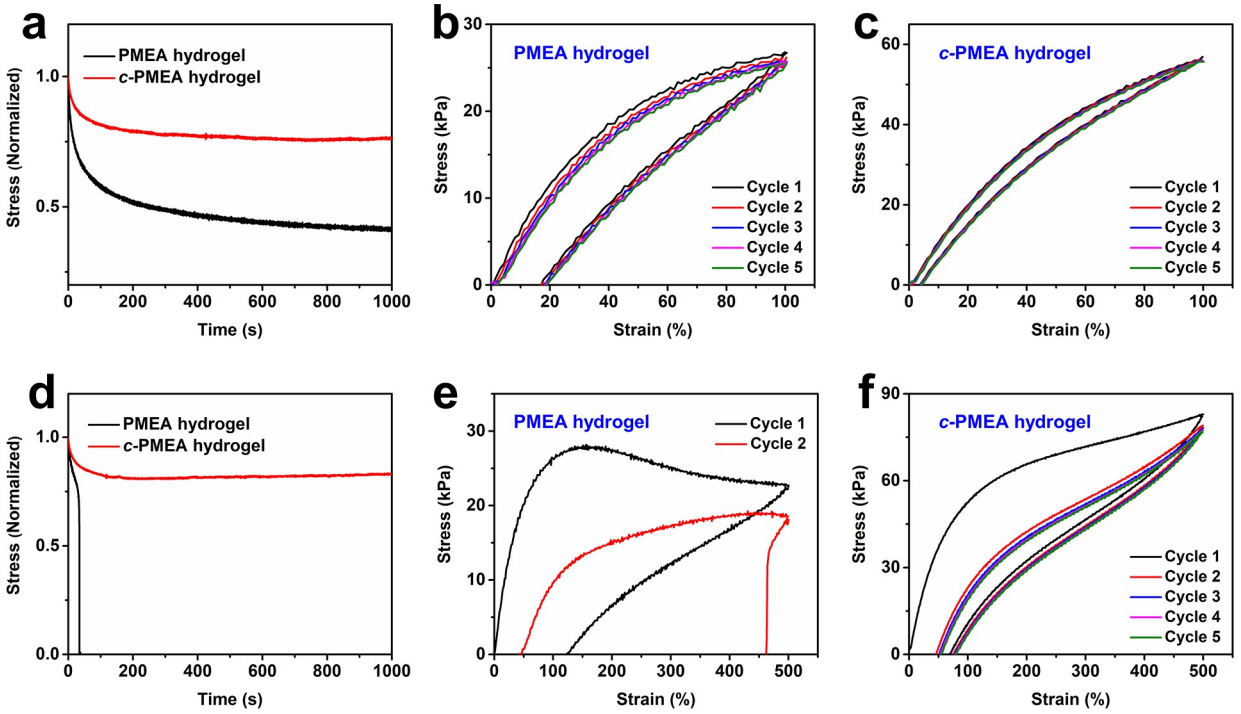

Figure 7. Stress relaxation and cyclic tensile tests of the PMEA and *c*-PMEA hydrogels. c_{AM} = 5 mol L^{-1} and $c_{micelle}$ = 1.2 mmol L^{-1}. Between each cycle, the hydrogel was rested for 5 min. (a) Stress relaxation behaviors of the PMEA and *c*-PMEA hydrogels under 100% strain. (b and c) Cyclic tensile tests of (b) the PMEA hydrogel and (c) the *c*-PMEA hydrogel under 100% strain. (d) Stress relaxation behaviors of the PMEA and *c*-PMEA hydrogels under 500% strain. (e and f) Cyclic tensile tests of (e) the PMEA hydrogel and (f) the *c*-PMEA hydrogel under 500% strain.

$$U_{hys} = U_{xl}\vartheta_e f_v, \quad (1)$$

where U_{xl} is the energy required for the detachment of block copolymer chains from the micellar core, ϑ_e is the concentration of elastically effective hydrophobic associations, and f_v is the fraction of broken hydrophobic association during the loading−unloading cycle.[51] According to eq 1, f_v increases with U_{hys} during the cyclic tensile tests, which means that the micellar crosslink is gradually broken as the strain increases.

Interestingly, both the hysteresis ratio and residual strain exhibit high dependence on the strain. As shown in Figure 5c, there are two distinctive dissipation processes divided by the critical yield strain (ε_y, ε_y = 200% according to the stress−strain curve) of the hydrogel, where the hysteresis ratio increases steeply before the yield point, while it increases slowly from 24 to 29% as the strain increases from 200 to 1000%. On the contrary, the residual strain increases slowly before the yield point, whereas it increases rapidly with the strain after the yield point.

To further clarify the energy dissipation mechanism, additional cyclic tensile tests were performed at 100 and 500% strains with a 5 min interval between each cycle. Whereas the hydrogel is elastic under 100% cyclic strain, with a recovery ratio of 100%, its recovery ratio is only 37% under 500% cyclic strain, suggesting the occurrence of irreversible energy dissipation (Figure 5d,e).[52] On the basis of the cyclic tensile tests and the energy dissipation mechanisms of micelle-crosslinked hydrogels, we propose the possible dissipative process of the micelle-crosslinked hydrogel, as in Figure 5f. Two main mechanisms are accounted for effective energy dissipation of micelle-crosslinked hydrogels, namely, the reversible deformation of micelles and irreversible removal of the block copolymer out of the micellar core.[16,22,53] When $\varepsilon < \varepsilon_y$, energy is dissipated by the reversible deformation of micelles. As the deformed micelles could recover quickly, the hydrogel exhibits elasticity with a high recovery ratio. When $\varepsilon > \varepsilon_y$, the block copolymers begin to detach from the micellar core, while the damaged crosslink cannot reform due to the slow and restrained dynamics of the block copolymers in hydrogels. Therefore, the hydrogel undergoes plastic deformation with a low recovery ratio and large residual strain.

Similar to cyclic tensile tests, the hydrogel also exhibits an obvious hysteresis loop upon cyclic compression to predetermined maximum strains, with the dissipated energy increasing with the maximum strain (Figure S9). Upon cyclic compression to a maximum strain of 70%, the hydrogel shows excellent fatigue resistance, while the hysteresis ratio remains unchanged within 10 cycles. Moreover, the recovery ratio is calculated to be 68%, indicating that the reversible deformation of micelles dominates the energy dissipation upon compressive stress.

Evaluation of PISA Library for Micelle-Crosslinked Hydrogels. Besides spherical micelles, PISA enables the design of polymeric assemblies of tailored morphology depending on the chain lengths of solvophilic and solvophobic blocks. To demonstrate the general applicability of polymeric assemblies to micelle-crosslinked hydrogels, $PDMAc_{50}$-*b*-$PDAAM_{500}$ vesicles were prepared via PISA of DAAM with $PDMAc_{50}$ as the macro-CTA. As shown in Figure 6a, DLS characterization reveals monodisperse particles with a hydrodynamic size of 254 nm (PDI = 0.032), while TEM confirmed their vesicular structure. After modification with vinyl groups, these vesicles were successfully applied to vesicle-crosslinked hydrogels. Mechanical tests indicate that the as-prepared hydrogels possess ultrastretchability and superior compressive properties, with ε_b = 2030% and $\sigma_{c,98\%}$ = 3.54 MPa (Figure 6a and Figure S10). Furthermore, the vesicle-crosslinked hydrogel

https://doi.org/10.1021/acs.chemmater.2c01001
Chem. Mater. 2022, 34, 6408−6419

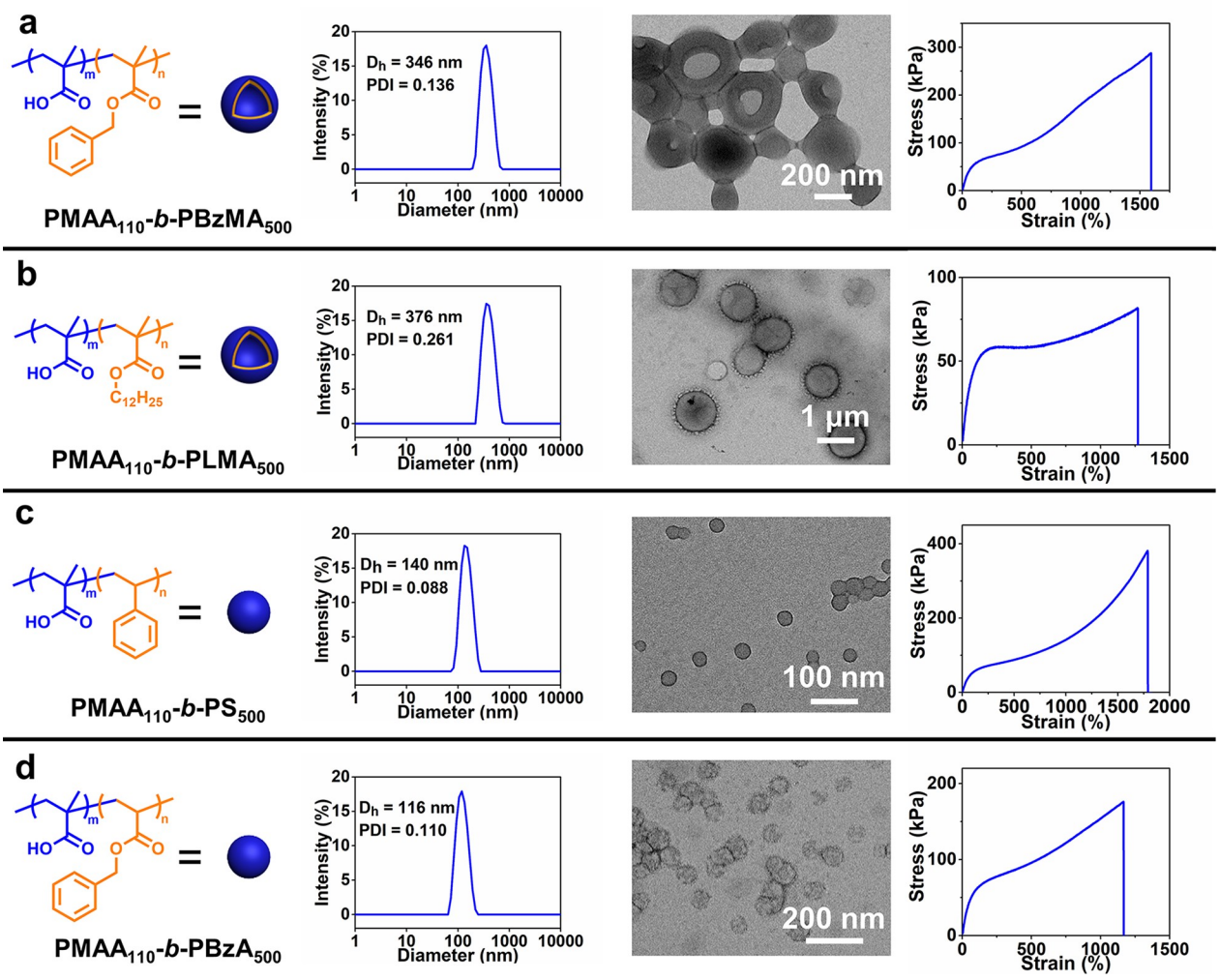

Figure 8. Summary of the alcoholic PISA formulations for micelle-crosslinked tough and ultrastretchable hydrogels. PISA of (a) $PMAA_{110}$-*b*-$PBzMA_{500}$, (b) $PMAA_{110}$-*b*-$PLMA_{500}$, (c) $PMAA_{110}$-*b*-PS_{500}, and (d) $PMAA_{110}$-*b*-$PBzA_{500}$ for micelle-crosslinked hydrogels. For each PISA formulation, the hydrodynamic size and morphology of the assemblies were characterized by DLS and TEM, and the mechanical property of the as-prepared hydrogel was characterized by a tensile test.

also exhibits an excellent fatigue resistance property under both cyclic tensile and compressive stress (Figure S11). Compared with micellar crosslinkers, the aqueous lumen of vesicular crosslinkers has been used to encapsulate drugs, enzymes, nanoparticles, etc.[40,54,55] Therefore, hydrogels crosslinked by vesicular crosslinkers may provide a new design of cargo-loaded hydrogels with a tunable release rate depending on the stress applied.

Besides the PISA of DAAM, the vast variety of aqueous PISA systems makes it possible to design and prepare micelle-crosslinked hydrogels with diverse chemical structures, mechanics, and functionalities. Three additional aqueous PISA formulations were evaluated for micelle-crosslinked hydrogels, including the aqueous PISA of 2-methoxyethyl acrylate (MEA),[56,57] 4-hydroxybutyl acrylate (HBA),[58] and tetrahydrofurfuryl acrylate (THFA)[58] (Figures S12−S15 and Table S2). As expected, these PISA formulations all afford micelles with a high concentration and uniform size dispersity, which all generate tough and ultrastretchable micelle-crosslinked hydrogels (Figure 6b−d and Figure S16). Notably, the mechanics of these hydrogels are correlated with the chemical composition of the micellar crosslinkers, with σ_b and toughness varied with the core-forming block. Furthermore, by comparing hydrogels crosslinked by $PDMAc_{100}$-*b*-$PMEA_{500}$ and $PDMAc_{100}$-*b*-$PTHFA_{500}$ micelles, one could find that on the premise of approximate concentration and diameter, micellar crosslinkers with a higher T_g of core-forming block would result in hydrogels with a higher σ_b, ε_b, and toughness (Table S3). According to the energy dissipative mechanism that we proposed in Figure 5f, we believe that the core-forming blocks of micellar crosslinkers are correlated with the mechanical properties of the hydrogels through the relaxation behavior of the micellar crosslinkers. The micelles with core-forming blocks of higher T_g have a slower relaxation process, which results in hydrogels with enhanced mechanics.

To verify our hypothesis, we prepared core-crosslinked PDMAc-*b*-PMEA micellar crosslinkers via PISA to restrict the interchain slippage in the micelles (Figure S17) and scrutinized the difference in mechanical properties of the hydrogels crosslinked with PDMAc-*b*-PMEA micelles and core-crosslinked PDMAc-*b*-PMEA micelles (denoted as PMEA hydrogel and *c*-PMEA hydrogel, respectively). As shown in Figure S18, the *c*-PMEA hydrogel shows profound strain hardening after yielding, with a σ_b of 242 kPa and an ε_b of 1830%. Compared with the PMEA hydrogel, the *c*-PMEA hydrogel shows a

https://doi.org/10.1021/acs.chemmater.2c01001
Chem. Mater. 2022, 34, 6408−6419

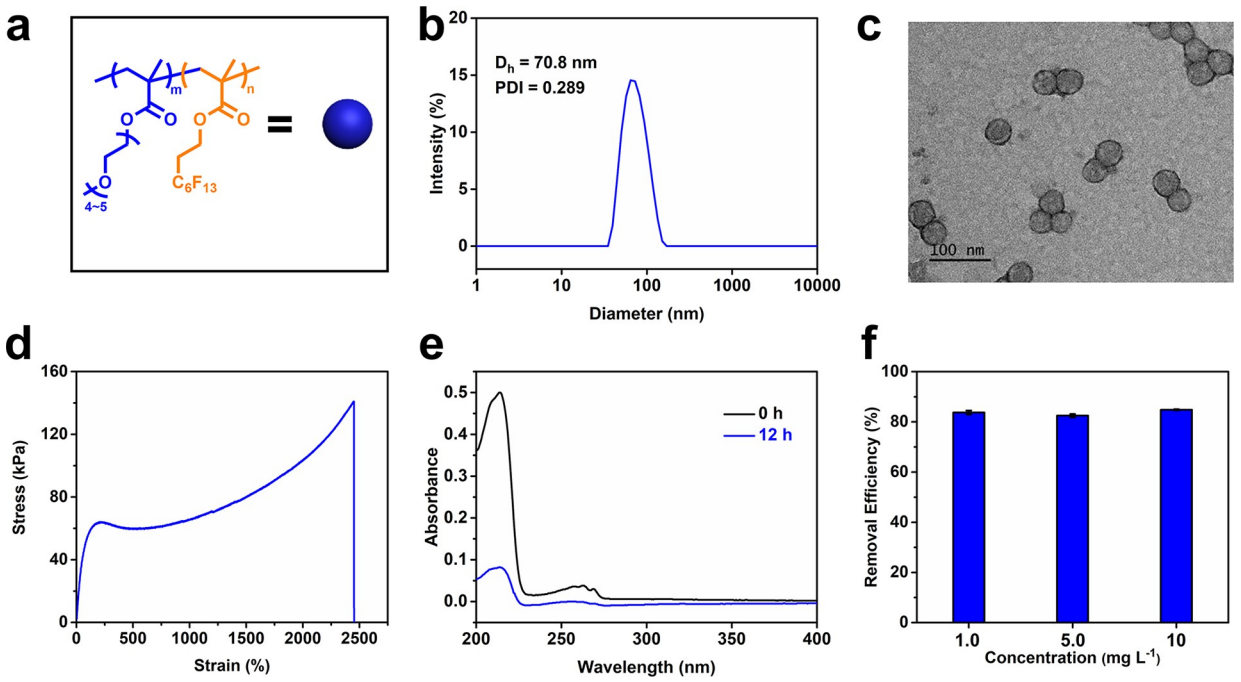

Figure 9. PISA of POEGMA$_{25}$-*b*-PFHEMA$_{50}$ for micelle-crosslinked fluoro-functionalized hydrogels. (a) Chemical composition, (b) hydrodynamic size, and (c) TEM image of the POEGMA$_{25}$-*b*-PFHEMA$_{50}$ micelles. (d) Tensile stress−strain curve of the hydrogel. (e) UV−Vis spectra of the fluoro-containing solution (10 mg L^{-1}) before and after the adsorption tests. (f) Removal efficiency of the hydrogel toward the fluoro-containing small molecule 4-(trifluoromethyl)benzyl alcohol.

significant improvement in strength (242 kPa vs 22.4 kPa) and toughness (2.10 MJ m^{-3} vs 0.353 MJ m^{-3}).

Stress relaxation and cyclic mechanical tests were performed to compare the relaxation behaviors of the PMEA and *c*-PMEA hydrogels. As shown in Figure 7a, under 100% strain, both PMEA and *c*-PMEA hydrogels reach new equilibrium within 1000 s, indicating the presence of crosslinks. The stress relaxation experiments are supported by the cyclic mechanical tests, in which both the PMEA and *c*-PMEA hydrogels exhibit good elasticity with high recovery ratios, suggesting the energy dissipation via reversible deformation of micelles (Figure 7b,c). Nevertheless, the *c*-PMEA hydrogel reserves a higher residual stress (75.9% vs 41.4%) and much lower hysteresis ratio (9.0% vs 34%) than the PMEA hydrogel, exhibiting superior elasticity.

Under 500% strain, the PMEA hydrogel ruptures within 35 s, suggesting rapid interchain slippage, whereas the *c*-PMEA hydrogel reaches new equilibrium in 1000 s and reserves 83% of the original internal stress (Figure 7d). In line with the stress relaxation tests, the PMEA hydrogel ruptures in the second cycle, while the *c*-PMEA hydrogel shows excellent fatigue resistance with a recovery ratio of 28%, suggesting that the irreversible rupture of the micelles contributes to the energy dissipation when $\varepsilon > \varepsilon_y$ (Figure 7e,f).

The PISA library for micelle-crosslinked hydrogels was subsequently extended to alcoholic systems (Figures S19−S24 and Table S4). As shown in Figure 8a−d and Figure S25, typical alcoholic PISA of methacrylates (benzyl methacrylate, BzMA;[35,59] lauryl methacrylate, LMA[60]), styrenics (styrene, St[61]), and acrylates (benzyl acrylate, BzA[62]) were all confirmed feasible to the preparation of micellar crosslinkers and micelle-crosslinked tough and ultrastretchable hydrogels. In view of the broad scope of PISA library, the development of micelle-crosslinked hydrogels would therefore be greatly promoted.

Modular Fabrication of Functional Micelle-Crosslinked Hydrogels via PISA. Besides the chemical composition and mechanics of the hydrogels, the functionality of micelle-crosslinked hydrogels could be modularly designed by tailoring the functionality of the micellar crosslinkers. To demonstrate this merit, fluoro-containing spherical micelles with a D_h of 70.8 nm were prepared by PISA of poly[oligo(ethylene glycol) methyl ether methacrylate]$_{25}$-*b*-poly[2-(perfluorohexyl)ethyl methacrylate]$_{50}$ (POEGMA$_{25}$-*b*-PFHEMA$_{50}$)[63,64] in EtOH/H$_2$O (85/15, wt/wt) with a solids content of 20 wt % (Figure 9a−f and Figures S26 and S27). After surface modification with vinyl groups, these micelles were copolymerized with AM to produce fluoro-containing hydrogels. Due to the strong and cooperative hydrophobic interaction of the fluoro-containing side chains, the hydrogels possess an ε_b of 2450% and a σ_b of 141 kPa, while their swelling ratio is as high as 16.2. The potential of this fluoro-containing hydrogel in adsorption of fluoro-containing molecules was further demonstrated by adsorption tests with 4-(trifluoromethyl)benzyl alcohol as the model compound. Removal efficiencies of 82.5−84.8% were achieved after soaking the fluoro-containing hydrogels in the aqueous solution of 4-(trifluoromethyl)benzyl alcohol of different concentrations (1.0, 5.0, and 10 mg L^{-1}) for 12 h. Therefore, we anticipate that this fluoro-containing hydrogel may be useful for remediation of fluoro-containing wastewater and controlled release of fluoro-containing pharmaceuticals.

CONCLUSIONS

To conclude, PISA was demonstrated to be a general and powerful platform for tough and ultrastretchable micelle-crosslinked hydrogels. Micellar crosslinkers with a high concentration, controlled nanostructure, and uniform size dispersity were synthesized via PISA and one-step post-

https://doi.org/10.1021/acs.chemmater.2c01001
Chem. Mater. 2022, 34, 6408−6419

polymerization modification and were subsequently copolymerized with acrylamide, generating hydrogels with superior toughness, ultrastretchability, and fatigue resistance. The mechanical properties of these hydrogels could be regulated by varying the concentration, size, and chemical composition of the micelles, and the energy dissipation mechanism was analyzed via stress relaxation and cyclic mechanical tests. The general feasibility of PISA for the rational design of micelle-crosslinked hydrogels was confirmed by systematic evaluation of both aqueous (including MEA, HBA, and THFA) and alcoholic (including BzMA, LMA, St, and BzA) PISA formulations. Such a broad library of PISA systems therefore enables the construction of functional micelle-crosslinked hydrogels with tailorable functionality, which was demonstrated by the fabrication of fluoro-containing hydrogels. Our work has significantly enlarged the scope of micelle-crosslinked hydrogels and further advances the exploration of micelle-crosslinked functional hydrogels.

EXPERIMENTAL SECTION

Synthesis of Polymeric Assemblies via Aqueous PISA. PDMAc-*b*-PDAAM diblock copolymer assemblies were synthesized via RAFT-mediated aqueous PISA with PDMAc as the corona-forming block. A typical procedure is depicted as follows: PDMAc macro-CTA (0.313 mmol, 3.13 g), DAAM (62.5 mmol, 10.6 g), and VA-044 (62.5 μmol, 20.0 mg) were weighed in a Schlenk tube, and H_2O (54.7 mL) was added. The solids content was 20 wt %. The sealed tube was degassed with N_2 for 30 min and was then placed into a preheated oil bath at 70 °C for 1 h. Afterward, the polymerization was quenched in iced water. ^{1}H NMR analysis indicated that the conversion of the polymerization was 99%. A portion was dried and characterized by ^{1}H NMR and SEC. The size and morphology of the sample were characterized by DLS and TEM.

With the same procedure, poly(*N*,*N*-dimethylacrylamide)-*b*-poly(2-methoxyethyl acrylate) (PDMAc-*b*-PMEA), poly(*N*,*N*-dimethylacrylamide)-*b*-poly(4-hydroxybutyl acrylate) (PDMAc-*b*-PHBA), and poly(*N*,*N*-dimethylacrylamide)-*b*-poly(tetrahydro-2-furanylmethyl acrylate) (PDMAc-*b*-PTHFA) assemblies were prepared using PDMAc as the macro-CTA.

Poly(methacrylic acid)-*b*-poly(benzyl methacrylate) (PMAA-*b*-PBzMA), poly(methacrylic acid)-*b*-poly(lauryl methacrylate) (PMAA-*b*-PLMA), poly(methacrylic acid)-*b*-poly(benzyl acrylate) (PMAA-*b*-PBzA), and poly(methacrylic acid)-*b*-polystyrene (PMAA-*b*-PS) assemblies were synthesized via RAFT-mediated alcoholic PISA with PMAA (M_n = 12,000 g mol^{-1}, $Đ$ = 1.23) as the corona-forming block. Poly[oligo(ethylene glycol) methyl ether methacrylate]-*b*-poly[2-(perfluorohexyl)ethyl methacrylate] (POEGMA-*b*-PFHEMA) assemblies were prepared by PISA in a mixture of ethanol and water (85/15, wt/wt). The solids content was 20 wt % for all the alcoholic PISA formulations.

Preparation of Micellar Crosslinkers via EDC Coupling. EDC (1.92 mmol, 0.368 g) and NHS (6.40 mmol, 0.737 g) were added to 60 mL of PDMAc-*b*-$PDAAM_{200}$ polymer assemblies ($c_{micelle}$ = 5.4 mmol L^{-1}), and the mixture was stirred for 2 h. Afterward, AEMA (4.80 mmol, 0.790 g) was added, and the mixture was adjusted to pH = 9 and was stirred for 24 h at room temperature. The reaction mixture was dialyzed against deionized water for 2 days to remove the impurities. The chemical structure of the micellar crosslinkers was verified by^1 H NMR.

Preparation of Micelle-Crosslinked Hydrogels. AM (3.02 g) and KPS (42.5 μmol, 11.5 mg) were mixed with the PDMAc-*b*-$PDAAM_{200}$ micellar crosslinker solution (0.84 mmol L^{-1}, 8.50 mL). The mixture was degassed with N_2 for 15 min under an ice bath. Afterward, the solution was injected into a 2 mm-thick rectangular silicone mold and a cylindrical mold and the polymerization was performed for 12 h at 50 °C. The detailed feed formulations for the micelle-crosslinked hydrogels are listed in Table S5.

Characterization of the Polymers. ^{1}H and ^{19}F nuclear magnetic resonance (NMR) spectra were recorded on a Bruker Avance II DMX (400 MHz for ^{1}H and 376 MHz for ^{19}F) spectrometer using $CDCl_3$ or DMSO-d_6 as the solvent. The molecular weights and dispersities ($Đ$) of polymers were characterized by a size exclusion chromatography (SEC) system at 35 °C, with DMF as an eluent at a flow rate of 1 mL min^{-1}. The SEC system is composed of a Waters 1525 isocratic HPLC pump, an Agilent PLgel 5 μm MIXED-C column, and a 2414 refractive index detector. Monodispersed polystyrene standards (M_p = 580−224,900 g mol^{-1}) were used for calibration.

Characterization of the Assemblies and Hydrogels. A HORIBA Delsa Nano equipped with a 633 nm He-Ne laser was used to characterize the hydrodynamic size of the assemblies. The scattering light at 90° angle was detected and used to analyze the size and size distribution. TEM images were obtained using a JEOL JEM-1400 Flash microscope operating at 120 kV. TEM samples were prepared by dropping 10 μL of sample onto a carbon-coated copper grid. After 1 min, the remaining solution was wiped off with blotting paper. The grid was further stained with 0.5 wt % phosphotungstic acid solution for 1 min. After removing the excess solution, the samples were dried under ambient conditions. SEM was performed on a Hitachi SU-8100 scanning electron microscope. The freeze-dried hydrogel samples were fractured in liquid nitrogen and fixed on the sample stage with conductive tape. The fractured cross section was sputtered with platinum for 90 s and was observed under an acceleration voltage of 15 kV.

Mechanical Testing. All mechanical tests were performed on a universal tensile tester (MOXIN MX-0350) equipped with a 50 N or 2000 N load cell. Uniaxial tensile tests were performed on dumbbell-shaped samples (gauge length: 12 mm (l_0) × 2 mm (w) × 2 mm (d)) at a rate of 100 mm min^{-1}. Compressive tests were performed on cylindrical samples with a diameter of 9 mm and a height of 10 mm at a crosshead speed of 10% strain per min. Samples were tested at least three times. The nominal stress (σ) was defined as $\sigma = F/S$, where F is the loading force applied to the sample and S is the initial cross-sectional area of the hydrogel sample. The nominal strain (ε) was determined by $\varepsilon = (l - l_0)/l_0$, where l is the gauge length during stretching and l_0 is the initial gauge length. Young's modulus was calculated by fitting the initial linear region of the stress−strain curve. The tensile toughness was estimated by the work of extension, which is calculated by integrating the area under the stress−strain curve.

For cyclic tests, the dumbbell-shaped hydrogels were stretched or compressed to predetermined maximum strain and then returned to their original length. The crosshead speed was 100 mm min^{-1} for cyclic tensile tests and 10% strain per min for cyclic compression tests. The U_{hys} was defined as the area of the hysteresis loop, and the hysteresis ratio was calculated by dividing the dissipated energy by the work of extension/compression:

$$U_{hys} = \int_{\varepsilon=0}^{\varepsilon=\varepsilon_x} (\sigma_{load} - \sigma_{unload}) d\varepsilon$$

$$\text{hysteresis ratio} = \int_{\varepsilon=0}^{\varepsilon=\varepsilon_x} \left(\frac{\sigma_{load} - \sigma_{unload}}{\sigma_{load}} \right) d\varepsilon \times 100\%$$

The recovery ratio was defined as the ratio of U_{hys} of cycle 2 to cycle 1:

$$\text{recovery ratio} = U_{hys}^{\text{cycle 2}} / U_{hys}^{\text{cycle 1}} \times 100\%$$

For stress relaxation tests, the dumbbell-shaped hydrogels were stretched to 100 or 500% strain at a rate of 100 mm min^{-1}, and the stress values were recorded until they reached an equilibrium.

ASSOCIATED CONTENT

Supporting Information

The Supporting Information is available free of charge at https://pubs.acs.org/doi/10.1021/acs.chemmater.2c01001.

https://doi.org/10.1021/acs.chemmater.2c01001
Chem. Mater. 2022, 34, 6408−6419

Full experimental details, synthetic diagrams and detailed structural characterizations of the micellar crosslinkers, formulations, and additional tensile and compressive tests for the micelle-crosslinked hydrogels (PDF)

AUTHOR INFORMATION

Corresponding Authors

Aiping Liu − *Center for Optoelectronics Materials and Devices, Key Laboratory of Optical Field Manipulation of Zhejiang Province, Zhejiang Sci-Tech University, Hangzhou 310018, China*; orcid.org/0000-0002-2338-062X; Email: liuaiping1979@gmail.com

Hailong Che − *Department of Chemical Engineering, School of Environmental and Chemical Engineering, Shanghai University, Shanghai 200444, China*; Email: hche@shu.edu.cn

Meng Huo − *Department of Chemistry, Key Laboratory of Surface & Interface Science of Polymer Materials of Zhejiang Province, Zhejiang Sci-Tech University, Hangzhou 310018, China; State Key Laboratory of Molecular Engineering of Polymers (Fudan University), Shanghai 200438, China*; orcid.org/0000-0001-8054-702X; Email: huomeng@zstu.edu.cn

Authors

Linlin Fan − *Department of Chemistry, Key Laboratory of Surface & Interface Science of Polymer Materials of Zhejiang Province, Zhejiang Sci-Tech University, Hangzhou 310018, China*

Zhong Zeng − *Department of Chemistry, Key Laboratory of Surface & Interface Science of Polymer Materials of Zhejiang Province, Zhejiang Sci-Tech University, Hangzhou 310018, China*

Ruixue Zhu − *Department of Chemistry, Key Laboratory of Surface & Interface Science of Polymer Materials of Zhejiang Province, Zhejiang Sci-Tech University, Hangzhou 310018, China*

Complete contact information is available at: https://pubs.acs.org/10.1021/acs.chemmater.2c01001

Notes

The authors declare no competing financial interest.

ACKNOWLEDGMENTS

This work was financially supported by the National Natural Science Foundation of China (grant no. 21905171), the Joint Funds of the Zhejiang Provincial Natural Science Foundation of China (grant no. LZY22E030002), and the Opening Project of the State Key Laboratory of Molecular Engineering of Polymers (Fudan University) (grant no. K2022-06). A.L. acknowledges the financial support from the Zhejiang Provincial Natural Science Foundation of China (grant no. LR19E020004) and the Youth Top-notch Talent Project of Zhejiang Ten Thousand Plan of China (no. ZJWR0308010).

REFERENCES

(1) Jungst, T.; Smolan, W.; Schacht, K.; Scheibel, T.; Groll, J. Strategies and molecular design criteria for 3D printable hydrogels. *Chem. Rev.* **2016**, *116*, 1496−1539.

(2) Means, A. K.; Grunlan, M. A. Modern Strategies To Achieve Tissue-Mimetic, Mechanically Robust Hydrogels. *ACS Macro Lett.* **2019**, *8*, 705−713.

(3) Wallin, T.; Pikul, J.; Shepherd, R. 3D printing of soft robotic systems. *Nat. Rev. Mater.* **2018**, *3*, 84−100.

(4) Du, X.; Zhai, J.; Li, X.; Zhang, Y.; Li, N.; Xie, X. Hydrogel-Based Optical Ion Sensors: Principles and Challenges for Point-of-Care Testing and Environmental Monitoring. *ACS Sens.* **2021**, *6*, 1990−2001.

(5) Yang, C.; Suo, Z. Hydrogel ionotronics. *Nat. Rev. Mater.* **2018**, *3*, 125−142.

(6) Zhang, Y. S.; Khademhosseini, A. Advances in engineering hydrogels. *Science* **2017**, *356*, No. eaaf3627.

(7) Zhao, X.; Chen, X.; Yuk, H.; Lin, S.; Liu, X.; Parada, G. Soft Materials by Design: Unconventional Polymer Networks Give Extreme Properties. *Chem. Rev.* **2021**, *121*, 4309−4372.

(8) Zhao, X. Multi-scale multi-mechanism design of tough hydrogels: building dissipation into stretchy networks. *Soft Matter* **2014**, *10*, 672−687.

(9) Bai, R.; Yang, J.; Suo, Z. Fatigue of hydrogels. *Eur. J. Mech. A. Solids* **2019**, *74*, 337−370.

(10) Gong, J. P.; Katsuyama, Y.; Kurokawa, T.; Osada, Y. Double-network hydrogels with extremely high mechanical strength. *Adv. Mater.* **2003**, *15*, 1155−1158.

(11) Xu, X.; Jerca, V. V.; Hoogenboom, R. Bioinspired double network hydrogels: from covalent double network hydrogels via hybrid double network hydrogels to physical double network hydrogels. *Mater. Horiz.* **2021**, *8*, 1173−1188.

(12) Wei, H.; Wang, Z.; Zhang, H.; Huang, Y.; Wang, Z.; Zhou, Y.; Xu, B. B.; Halila, S.; Chen, J. Ultrastretchable, Highly Transparent, Self-Adhesive, and 3D-Printable Ionic Hydrogels for Multimode Tactical Sensing. *Chem. Mater.* **2021**, *33*, 6731−6742.

(13) Haraguchi, K.; Takehisa, T. Nanocomposite hydrogels: A unique organic−inorganic network structure with extraordinary mechanical, optical, and swelling/de-swelling properties. *Adv. Mater.* **2002**, *14*, 1120−1124.

(14) Zhao, Z.; Fang, R.; Rong, Q.; Liu, M. Bioinspired nanocomposite hydrogels with highly ordered structures. *Adv. Mater.* **2017**, *29*, 1703045.

(15) Yu, X.; Zheng, Y.; Zhang, H.; Wang, Y.; Fan, X.; Liu, T. Fast-Recoverable, Self-Healable, and Adhesive Nanocomposite Hydrogel Consisting of Hybrid Nanoparticles for Ultrasensitive Strain and Pressure Sensing. *Chem. Mater.* **2021**, *33*, 6146−6157.

(16) Fu, J. Strong and tough hydrogels crosslinked by multifunctional polymer colloids. *J. Polym. Sci., Part B: Polym. Phys.* **2018**, *56*, 1336−1350.

(17) Huang, T.; Xu, H.; Jiao, K.; Zhu, L.; Brown, H. R.; Wang, H. A novel hydrogel with high mechanical strength: a macromolecular microsphere composite hydrogel. *Adv. Mater.* **2007**, *19*, 1622−1626.

(18) Xiao, L.; Liu, C.; Zhu, J.; Pochan, D. J.; Jia, X. Hybrid, elastomeric hydrogels crosslinked by multifunctional block copolymer micelles. *Soft Matter* **2010**, *6*, 5293−5297.

(19) Wang, P.; Deng, G.; Zhou, L.; Li, Z.; Chen, Y. Ultrastretchable, Self-Healable Hydrogels Based on Dynamic Covalent Bonding and Triblock Copolymer Micellization. *ACS Macro Lett.* **2017**, *6*, 881−886.

(20) Song, M.-M.; Wang, Y.-M.; Wang, B.; Liang, X.-Y.; Chang, Z.-Y.; Li, B.-J.; Zhang, S. Super tough, ultrastretchable hydrogel with multistimuli responsiveness. *ACS Appl. Mater. Interfaces* **2018**, *10*, 15021−15029.

(21) Qin, Z.; Yu, X.; Wu, H.; Li, J.; Lv, H.; Yang, X. Nonswellable and tough supramolecular hydrogel based on strong micelle cross-linkings. *Biomacromolecules* **2019**, *20*, 3399−3407.

(22) Xiao, L.; Zhu, J.; Londono, J. D.; Pochan, D. J.; Jia, X. Mechano-responsive hydrogels crosslinked by block copolymer micelles. *Soft Matter* **2012**, *8*, 10233−10237.

(23) Yu, X.; Qin, Z.; Wu, H.; Lv, H.; Yang, X. Tuning hydrogel mechanics by kinetically dependent cross-linking. *Macromolecules* **2019**, *52*, 1249−1256.

(24) Sun, Y.; Liu, S.; Du, G.; Gao, G.; Fu, J. Multi-responsive and tough hydrogels based on triblock copolymer micelles as multifunctional macro-crosslinkers. *Chem. Commun.* **2015**, *51*, 8512−8515.

(25) Sun, Y.-n.; Gao, G.-r.; Du, G.-l.; Cheng, Y.-j.; Fu, J. Super tough, ultrastretchable, and thermoresponsive hydrogels with functionalized triblock copolymer micelles as macro-cross-linkers. *ACS Macro Lett.* **2014**, *3*, 496−500.
(26) Yu, X.; Qin, Z.; Wu, H.; Lv, H.; Yang, X. pH-driven preparation of small, non-aggregated micelles for ultra-stretchable and tough hydrogels. *Chem. Eng. J.* **2018**, *342*, 357−363.
(27) Ren, P.; Zhang, H.; Dai, Z.; Ren, F.; Wu, Y.; Hou, R.; Zhu, Y.; Fu, J. Stiff micelle-crosslinked hyaluronate hydrogels with low swelling for potential cartilage repair. *J. Mater. Chem. B* **2019**, *7*, 5490−5501.
(28) Fang, K.; Wang, R.; Zhang, H.; Zhou, L.; Xu, T.; Xiao, Y.; Zhou, Y.; Gao, G.; Chen, J.; Liu, D.; Ai, F.; Fu, J. Mechano-Responsive, Tough, and Antibacterial Zwitterionic Hydrogels with Controllable Drug Release for Wound Healing Applications. *ACS Appl. Mater. Interfaces* **2020**, *12*, 52307−52318.
(29) Sun, P.; Zhang, H.; Xu, D.; Wang, Z.; Wang, L.; Gao, G.; Hossain, G.; Wu, J.; Wang, R.; Fu, J. Super tough bilayer actuators based on multi-responsive hydrogels crosslinked by functional triblock copolymer micelle macro-crosslinkers. *J. Mater. Chem. B* **2019**, *7*, 2619−2625.
(30) Wu, M.; Chen, J.; Ma, Y.; Yan, B.; Pan, M.; Peng, Q.; Wang, W.; Han, L.; Liu, J.; Zeng, H. Ultra elastic, stretchable, self-healing conductive hydrogels with tunable optical properties for highly sensitive soft electronic sensors. *J. Mater. Chem. A* **2020**, *8*, 24718−24733.
(31) Mai, Y.; Eisenberg, A. Self-assembly of block copolymers. *Chem. Soc. Rev.* **2012**, *41*, 5969−5985.
(32) Wang, X.; Shen, L.; An, Z. Dispersion polymerization in environmentally benign solvents via reversible deactivation radical polymerization. *Prog. Polym. Sci.* **2018**, *83*, 1−27.
(33) Warren, N. J.; Armes, S. P. Polymerization-induced self-assembly of block copolymer nano-objects via RAFT aqueous dispersion polymerization. *J. Am. Chem. Soc.* **2014**, *136*, 10174−10185.
(34) Liu, C.; Hong, C.-Y.; Pan, C.-Y. Polymerization techniques in polymerization-induced self-assembly (PISA). *Polym. Chem.* **2020**, *11*, 3673−3689.
(35) Gonzato, C.; Semsarilar, M.; Jones, E. R.; Li, F.; Krooshof, G. J.; Wyman, P.; Mykhaylyk, O. O.; Tuinier, R.; Armes, S. P. Rational synthesis of low-polydispersity block copolymer vesicles in concentrated solution via polymerization-induced self-assembly. *J. Am. Chem. Soc.* **2014**, *136*, 11100−11106.
(36) d'Agosto, F.; Rieger, J.; Lansalot, M. RAFT-Mediated Polymerization-Induced Self-Assembly. *Angew. Chem., Int. Ed.* **2020**, *59*, 8368−8392.
(37) Canning, S. L.; Smith, G. N.; Armes, S. P. A critical appraisal of RAFT-mediated polymerization-induced self-assembly. *Macromolecules* **2016**, *49*, 1985−2001.
(38) Morimura, M.; Ida, S.; Oyama, M.; Takeshita, H.; Kanaoka, S. Design of Hydrogels with Thermoresponsive Crosslinked Domain Structures via the Polymerization-Induced Self-Assembly Process and Their Thermoresponsive Toughening in Air. *Macromolecules* **2021**, *54*, 1732−1741.
(39) Deane, O. J.; Jennings, J.; Neal, T. J.; Musa, O. M.; Fernyhough, A.; Armes, S. P. Synthesis and Aqueous Solution Properties of Shape-Shifting Stimulus-Responsive Diblock Copolymer Nano-Objects. *Chem. Mater.* **2021**, *33*, 7767−7779.
(40) Du, Y.; Jia, S.; Chen, Y.; Zhang, L.; Tan, J. Type I Photoinitiator-Functionalized Block Copolymer Nanoparticles Prepared by RAFT-Mediated Polymerization-Induced Self-Assembly. *ACS Macro Lett.* **2021**, *10*, 297−306.
(41) Penfold, N. J. W.; Yeow, J.; Boyer, C.; Armes, S. P. Emerging Trends in Polymerization-Induced Self-Assembly. *ACS Macro Lett.* **2019**, *8*, 1029−1054.
(42) Lv, F.; An, Z.; Wu, P. Scalable preparation of alternating block copolymer particles with inverse bicontinuous mesophases. *Nat. Commun.* **2019**, *10*, 1397.
(43) Byard, S. J.; Williams, M.; McKenzie, B. E.; Blanazs, A.; Armes, S. P. Preparation and Cross-Linking of All-Acrylamide Diblock Copolymer Nano-Objects via Polymerization-Induced Self-Assembly in Aqueous Solution. *Macromolecules* **2017**, *50*, 1482−1493.
(44) Zhou, W.; Qu, Q.; Xu, Y.; An, Z. Aqueous polymerization-induced self-assembly for the synthesis of ketone-functionalized nano-objects with low polydispersity. *ACS Macro Lett.* **2015**, *4*, 495−499.
(45) Moad, G.; Chen, M.; Häussler, M.; Postma, A.; Rizzardo, E.; Thang, S. H. Functional polymers for optoelectronic applications by RAFT polymerization. *Polym. Chem.* **2011**, *2*, 492−519.
(46) Keddie, D. J.; Moad, G.; Rizzardo, E.; Thang, S. H. RAFT agent design and synthesis. *Macromolecules* **2012**, *45*, 5321−5342.
(47) Jones, E.; Mykhaylyk, O.; Semsarilar, M.; Boerakker, M.; Wyman, P.; Armes, S. How do spherical diblock copolymer nanoparticles grow during RAFT alcoholic dispersion polymerization? *Macromolecules* **2016**, *49*, 172−181.
(48) Derry, M. J.; Fielding, L. A.; Warren, N. J.; Mable, C. J.; Smith, A. J.; Mykhaylyk, O. O.; Armes, S. P. In situ small-angle X-ray scattering studies of sterically-stabilized diblock copolymer nanoparticles formed during polymerization-induced self-assembly in non-polar media. *Chem. Sci.* **2016**, *7*, 5078−5090.
(49) Czajka, A.; Armes, S. P. In situ SAXS studies of a prototypical RAFT aqueous dispersion polymerization formulation: monitoring the evolution in copolymer morphology during polymerization-induced self-assembly. *Chem. Sci.* **2020**, *11*, 11443−11454.
(50) Gu, Y.; Zhao, J.; Johnson, J. A. A (Macro)Molecular-Level Understanding of Polymer Network Topology. *Trends Chem.* **2019**, *1*, 318−334.
(51) Tuncaboylu, D. C.; Sahin, M.; Argun, A.; Oppermann, W.; Okay, O. Dynamics and Large Strain Behavior of Self-Healing Hydrogels with and without Surfactants. *Macromolecules* **2012**, *45*, 1991−2000.
(52) Tang, J.; Xu, G.; Sun, Y.; Pei, Y.; Fang, D. Dissipative properties and chain evolution of highly strained nanocomposite hydrogel. *J. Appl. Phys.* **2014**, *116*, 244901.
(53) Xu, Z.; Li, J.; Gao, G.; Wang, Z.; Cong, Y.; Chen, J.; Yin, J.; Nie, L.; Fu, J. Tough and self-recoverable hydrogels crosslinked by triblock copolymer micelles and Fe^{3+} coordination. *J. Polym. Sci., Part B: Polym. Phys.* **2018**, *56*, 865−876.
(54) Blackman, L. D.; Varlas, S.; Arno, M. C.; Fayter, A.; Gibson, M. I.; O'Reilly, R. K. Permeable protein-loaded polymersome cascade nanoreactors by polymerization-induced self-assembly. *ACS Macro Lett.* **2017**, *6*, 1263−1267.
(55) Mable, C. J.; Gibson, R. R.; Prevost, S.; McKenzie, B. E.; Mykhaylyk, O. O.; Armes, S. P. Loading of silica nanoparticles in block copolymer vesicles during polymerization-induced self-assembly: Encapsulation efficiency and thermally triggered release. *J. Am. Chem. Soc.* **2015**, *137*, 16098−16108.
(56) Liu, G.; Qiu, Q.; Shen, W.; An, Z. Aqueous Dispersion Polymerization of 2-Methoxyethyl Acrylate for the Synthesis of Biocompatible Nanoparticles Using a Hydrophilic RAFT Polymer and a Redox Initiator. *Macromolecules* **2011**, *44*, 5237−5245.
(57) Mellot, G.; Guigner, J.-M.; Bouteiller, L.; Stoffelbach, F.; Rieger, J. Templated PISA: Driving Polymerization-Induced Self-Assembly towards Fibre Morphology. *Angew. Chem., Int. Ed.* **2019**, *58*, 3173−3177.
(58) Foster, J. C.; Varlas, S.; Couturaud, B.; Jones, J. R.; Keogh, R.; Mathers, R. T.; O'Reilly, R. K. Predicting Monomers for Use in Polymerization-Induced Self-Assembly. *Angew. Chem., Int. Ed.* **2018**, *57*, 15733−15737.
(59) Semsarilar, M.; Jones, E. R.; Blanazs, A.; Armes, S. P. Efficient Synthesis of Sterically-Stabilized Nano-Objects via RAFT Dispersion Polymerization of Benzyl Methacrylate in Alcoholic Media. *Adv. Mater.* **2012**, *24*, 3378−3382.
(60) Gibson, R. R.; Cornel, E. J.; Musa, O. M.; Fernyhough, A.; Armes, S. P. RAFT dispersion polymerisation of lauryl methacrylate in ethanol−water binary mixtures: synthesis of diblock copolymer vesicles with deformable membranes. *Polym. Chem.* **2020**, *11*, 1785−1796.

https://doi.org/10.1021/acs.chemmater.2c01001
Chem. Mater. 2022, 34, 6408−6419

(61) Wan, W.-M.; Hong, C.-Y.; Pan, C.-Y. One-pot synthesis of nanomaterials via RAFT polymerization induced self-assembly and morphology transition. *Chem. Commun.* **2009**, *45*, 5883−5885.
(62) Tkachenko, V.; Kunemann, P.; Malval, J. P.; Petithory, T.; Pieuchot, L.; Vidal, L.; Chemtob, A. Kinetically stable sub-50 nm fluorescent block copolymer nanoparticles via photomediated RAFT dispersion polymerization for cellular imaging. *Nanoscale* **2022**, *14*, 534−545.
(63) Huo, M.; Li, D.; Song, G.; Zhang, J.; Wu, D.; Wei, Y.; Yuan, J. Semi-Fluorinated Methacrylates: A Class of Versatile Monomers for Polymerization-Induced Self-Assembly. *Macromol. Rapid Commun.* **2018**, *39*, 1700840.
(64) Huo, M.; Zeng, M.; Li, D.; Liu, L.; Wei, Y.; Yuan, J. Tailoring the multicompartment nanostructures of fluoro-containing ABC triblock terpolymer assemblies via polymerization-induced self-assembly. *Macromolecules* **2017**, *50*, 8212−8220.

https://doi.org/10.1021/acs.chemmater.2c01001
Chem. Mater. 2022, 34, 6408−6419